Journal of Analytical and Applied Pyrolysis 134 (2018) 326–335

Contents lists available at ScienceDirect

Journal of Analytical and Applied Pyrolysis

journal homepage: www.elsevier.com/locate/jaap

A predictive model of biochar formation and characterization

P. Debiagi, G. Gentile, A. Cuoci, A. Frassoldati, E. Ranzi, T. Faravelli*

CRECK Modeling Group, Dipartimento di Chimica, Materiali e Ingegneria Chimica "Giulio Natta", Politecnico di Milano, Piazza Leonardo Da Vinci, 32, 20133 Milano, Italy

ARTICLE INFO

Keywords:
Biochar
Pyrolysis
Biomass
Kinetic mechanism
Solid fuel

ABSTRACT

Biomass is increasingly being recognized as a promising carrier for both heat, energy and chemicals production. However, several aspects still require intense research activity towards a better design and optimization of industrial combustors, gasifiers and pyrolyzer. The objective of this work is to update the CRECK kinetic mechanism of biomass pyrolysis, allowing a better prediction of both yield and composition of the solid residue (biochar). Moreover, further model modifications allow to better describe the variability of hemicellulose in different biomass. To this end, a large set of literature experimental data is collected and organized into a database, which is used to further tune and validate the proposed kinetic mechanism. Although the kinetic model maintains the previous agreement in respect of the rate of biomass pyrolysis, formation and distribution of gas and tar products, the novelty of this work is the greater attention to the predictions of biochar yield and composition, in a wide range of operative conditions. The model describes the solid residue as a mixture of pure carbon together with lumped metaplastic compounds, which represent the whole range of oxygenated and hydrogenated groups bonded to the carbonaceous matrix. These metaplastic species are released to the gas phase with their own kinetics and describe the change of both mass loss and elemental composition of the biochar. These comprehensive predictions of biochar composition are crucial for an accurate description of the successive oxidation and gasification processes.

1. Introduction

Modern world energy demand is yet highly dependent on fossil fuels availability, which is threaten by their intensive and increasing consumption [1]. The volatility of petrol market, together with environmental pollution and specially greenhouse effect, are paving the way to explore new and renewable energy sources [1–3].

In this context, interest is increasing towards biomass as a renewable source of fuels. They are worldwide available, produce negligible CO_2 emissions compared to fossil fuels and can be harvested from underrated crops, manure and wood processing residues. Wood, plants, agriculture and forest residues, and also most of non-animal food processing industries residues are classified as lignocellulosic biomass. These are the most common and available biomass feedstock, which can be converted to eligible fuels such as methane via anaerobic digestion, ethanol via fermentation, green diesel and gasoline replacements via hydrothermal conversion or even bio-oil, syngas and biochar via thermochemical conversion [4]. Multiple and complex products can be obtained through the thermochemical route [5] which is the route investigated in the present work.

The first step of biomass thermochemical conversion is the pyrolysis, in which the material is heated under inert atmosphere, releasing the volatile matter from the raw material, yielding solid biochar, condensable tar, and gas [6]. Slow pyrolysis, in particular, is a suitable alternative when high yields of the solid product are requested. At temperatures not higher than 650 K, with slow heating rates and long residence times (hours), this process gives yields up to 50 wt.% of biochar. Biomass isolated compounds produce biochar in different amounts. The lowest yield is for cellulose, followed by hemicellulose and lignin, which reaches up to 50% of its initial weight [7]. Because of a catalytic effect, inorganic matter in larger amounts increase solid and gases yields, consequently reducing bio-oil yields [8].

The solid residue is an amorphous carbon structure containing significant amounts of oxygen and hydrogen, a minor amount of nitrogen and sulfur, together with metal oxides (i.e. ashes), which are formed from the inorganic matter present in the raw material during pyrolysis. The carbon content usually ranges from 65 to 95% depending on the initial biomass composition and pyrolysis operating conditions. Hydrogen and oxygen contents progressively drop when pyrolysis temperature rises. Their content directly influences biochar conversion during oxidation and gasification processes. In particular, H and O sites disturb the organization of the crystalline carbon matrix with the

* Corresponding author.
E-mail address: tiziano.faravelli@polimi.it (T. Faravelli).

https://doi.org/10.1016/j.jaap.2018.06.022
Received 3 May 2018; Received in revised form 14 June 2018; Accepted 19 June 2018
Available online 28 June 2018

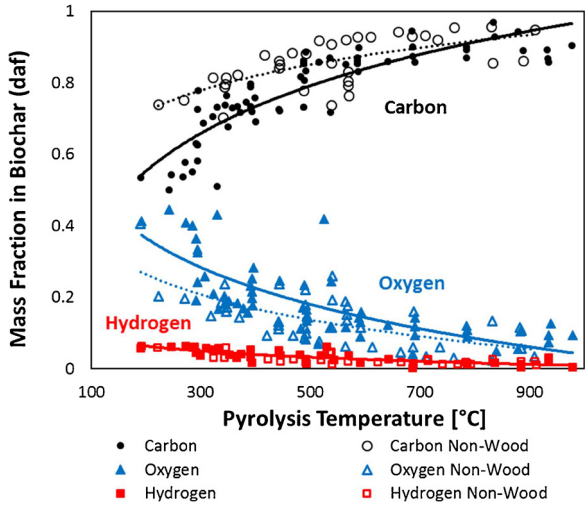

Fig. 1. Elemental C/O/H composition of dry ash-free biochar as a function of the pyrolysis peak temperature. Dashed lines are given in Eqs. (2)–(4). Open symbols: wood. Solid symbol: non-wood. After Neves, et al. [11].

formation of amorphous areas and weakly bonded functional groups. These factors enhance the surface area, the amount of volatile matter in the biochar and the density of surface active sites, thus conditioning biochar reactivity. Although char from coal at high temperatures (T > 1000-1200 °C) can undergo a progressive graphitization [9], this annealing process should be less relevant for biochar, because of its higher reactivity and less severe operating conditions. Moreover, the operating conditions analyzed in the present work do not fall into the annealing severity conditions. On the contrary, heterogeneous secondary reactions during slow pyrolysis can strongly affect biochar reactivity, mainly in case of large particles [10].

Neves, et al. [11] extensively analyzed the characterization and prediction of biomass pyrolysis products, with particular attention to the residual biochar. They also derived empirical relationships from the collected data, considering a variety of fuels over a wide range of pyrolysis conditions, including relations between the yields of gas-phase volatiles and thermochemical properties of char, tar and gas.

Fig. 1 shows the elemental composition of dry ash free biochar, in terms of C, H and O, as a function of the pyrolysis peak temperature. The elemental composition varies roughly from the one of the parent fuel to about 100% carbon, being highly dependent on the pyrolysis temperature. The carbon content of biochar increases with temperature increase, meanwhile there is a loss of oxygen and hydrogen. Typically, the amount of O decreases from 20 to 40 to 5–10%, while the H content is lower than 1–2%. The investigation divided the samples into wood (raw and residues of wood) and non-wood biomass (grasses, cereals, residues from agriculture and industry processes). The lines in Fig. 1 show the predictions of an exponential correlation distinguishing the two sub-set of samples and they indicate a tendency of non-wood biomasses to generate chars with higher carbon content. This fact can be at least partially explained by the higher carbon of the parent fuel, and elevated ash matter that promotes dehydration reactions by catalytic effect of the inorganics. On the other hand, Neves, et al. [11] proposed these all-inclusive temperature-dependent regressions for the yield of char and for its composition in terms of C, H, and O mass fractions, in the temperature range of 250–1000 °C:

$$Y_{Char} = 0.106 + 2.43 \cdot e^{-0.0066 \cdot T} \quad R^2 = 0.56 \tag{1}$$

$$Y_C = 0.93 - 0.92 \cdot e^{-0.0042 \cdot T} \quad R^2 = 0.65 \tag{2}$$

$$Y_O = 0.07 + 0.85 \cdot e^{-0.0048 \cdot T} \quad R^2 = 0.56 \tag{3}$$

$$Y_H = -0.0041 + 0.1 \cdot e^{-0.0024 \cdot T} \quad R^2 = 0.75 \tag{4}$$

The large scatter of the data and the poor correlation indexes, can be improved by considering wood and non-wood fuels, as reported in Fig. 1. Indeed, not only the parent biomass atomic composition and the peak temperature but also operating conditions strongly influence the pyrolysis process. Biochemical composition, heating rate and peak temperature are the most influencing process conditions [10,11].

As already observed by Anca-Couce [12], at low temperatures (< 800 K) and low heating rates most of the volatiles have been already released and char and tar are the most abundant products, whereas the gas yield is lower. When charring is promoted, as in slow pyrolysis or when a high ash content acts as catalyst, total tar yield is reduced while the yields of char, CO_2 and H_2O are enhanced. At higher temperatures (> 800 K), the CO and H2 yields increase drastically, while tar and char yields are reduced. This is due both to secondary decomposition reactions of tar species and also to the progressive char devolatilization processes. Thus, higher heating rates promote production of higher liquid yields, whereas lower heating rates enhance biochar formation. Higher amounts of cellulose favor bio-oil production and higher lignin contents enhance biochar yields. The optimum temperature for the maximum bio-oil yield is in the range of 650–800 K [5]. Reaction atmosphere and residence time both significantly affect the biochar composition and the pyrolysis products. Further modifications in the pyrolysis process can also be due to biomass pretreatments [13].

A multistep model of biomass pyrolysis needs to account for both the primary pyrolysis of reference components as well as successive char devolatilization reactions, through the progressive release of metaplastic species. Moreover, secondary tar cracking processes, as well as secondary cross-linking processes require a model at the particle and reactor scale [14].

The aim of this work is to discuss the performances of CRECK kinetic model of biomass pyrolysis [5] mainly with respect to the formation of biochar in terms of both yield and H/C/O elemental composition, for different biomass feedstocks and for a wide range of pyrolysis conditions.

As a first step of this research activity, a large set of literature experimental data was collected and organized in a database, which is available in the Supplemental Material (SM). These data, partially collected from the previous referred review paper [11] as well as from more recent sources properly referred in the SM, show a large variability of the residual biochar yield and its H/C/O elemental composition for the whole set of biomass samples at different pyrolysis temperatures and conditions. This database contains the composition of the parent biomass, the pyrolysis conditions, the yield and composition of the residual biochar. Other biochar physical properties and structural characteristics are also reported, when available.

The biochar yield and its composition cannot be simply related to pyrolysis peak temperature. This variability also depends on initial biomass composition, heating rate, hold time, and other process conditions. Moreover, ash catalytic effects and secondary charification reactions [15] can further influence this complex scenario.

According to Gómez-Barea and Leckner [16], the conversion of tar components is below 10 wt.% at low temperatures (up to 500 °C) and gas retention times lower than 0.5 s. Thus, experiments with thin particles (sizes < 100–300 μm) [17] are referred as micro experiments. In those cases, heat and mass transfer limitations, as well as secondary gas-phase reactions can be neglected. Only those data referring to micro-experiments, and containing enough details on biomass composition and operating conditions to allow a proper simulation were processed and analyzed in the successive discussion. As a consequence, the comparison with the literature data is limited to a fraction of the whole set of experimental data collected in the database.

This work is structured in the following way: Section 2 presents and discusses the CRECK kinetic mechanism of biomass pyrolysis, which was further tuned and validated, mainly in order to improve model predictions of biochar yield and composition, still maintaining the previous agreement with the whole set of experimental data [18].

Detailed comparisons of predicted and experimental measurements are reported for a few examples, mainly referred to hemicellulose pyrolysis. In fact, the updated kinetic model allows to distinguish the different nature of hemicellulose in softwood, hardwood, and grass/cereal samples. Section 3 analyzes the model performances mainly in terms the parity diagrams of biochar yields, as well as carbon, oxygen, and hydrogen composition. Model predictions allow to drastically improve the correlation indexes of the previous Eqs. (1)–(4). All these data and simulation examples refer only to thin or fine biomass particles, where internal mass and heat transfer resistances are not significant and then secondary charification reactions of tar species are not considered [12]. Finally, Section 4 and the Conclusion present some considerations on the sensitivity of the model to the rate parameters and highlight the possibilities and limitations of the biomass pyrolysis model in predicting the yield and composition of biochar.

2. Multistep kinetic mechanism of biomass pyrolysis

The detailed pyrolysis model applied in this work is based on the lumped one originally proposed and recently updated by Ranzi et al. [5,19]. When biochemical composition is not available, biomass samples are characterized on the basis of their elemental analysis. The C, H and O content allows to estimate the biomass composition in terms of cellulose, hemicellulose, lignins, and extractives. As already discussed in previous papers, the pyrolysis of biomass can be considered as a linear combination of the decomposition of cellulose (CELL), hemicellulose (GMSW/ XYHW/XYGR), lignin (LIG-C, LIG-H and LIG-O) and extractives (TANN and TGL) [18]. Because of its variability in elemental composition, lignin is characterized in terms of three reference components (LIG-C, LIG-H and LIG-O) [20].

The different plots in Fig. 2 show examples of the global features of this multistep kinetic model. It refers to the pyrolysis of a cereal biomass sample and compares model predictions with the experimental data of a thermo-gravimetric analysis (TGA) [21]. Along with the comparison between the experimental and predicted TGA and DTG (panel a), the model describes the release of main gas and condensable components (panel b). The resulting evolution of the elemental composition of biochar, in terms of carbon, hydrogen and oxygen content is also predicted (panel c). This figure also highlights the three successive phases of dehydration, pyrolysis of main biomass components, and the progressive and final gas and tar release from the species trapped in the metaplastic phase.

As already discussed in previous paper [22], it is important to underline that the kinetic model of biomass pyrolysis is and has been progressively modified in order to continuously account for new available experimental data. For instance, the modifications of the thermochemistry and reaction heats [23], allowed us to better investigate the low temperature experimental activity on biochar formation [24]. Moreover, detailed time resolved species concentration profiles allowed to further tune and modify the overall stoichiometries. Similarly, the modifications related to the catalytic effect of ash [5] were made without relevant effects on the whole set of previous validations. Very recently, Dussan, et al. [25] investigated the kinetic mechanism of hemicellulose pyrolysis. They chose five model compounds, xylan cluster (xylan with acetyl and 4-methyl-D-glucuronic acid groups), arabinoxylan, xyloglucan, glucomannan, and β-glucan, to replicate the carbohydrate structural features of three typical biomass categories (softwoods, hardwoods and grass/herbaceous plants). They also proposed a series of lumped pyrolysis reactions with global stoichiometries and rate constants that are numerically optimized to reproduce a large series of experimental data. Taking advantage of this study, we improved the description of hemicellulose in the CRECK pyrolysis mechanism by using simply two reference components: HCE1 and HCE2. Three different combinations of these two reference components allow to distinguish hemicellulose in softwood (GMSW, mainly representative of glucomannan: HCE1/HCE2 = 70/30), hardwood (XYHW, representative of arabinoxylan: HCE1/HCE2 = 35/65), and Grass/Cereal (XYGR: HCE1/HCE2 = 12/88) feedstocks.

Then, the major modifications of the revised mechanism discussed in this work refer to the hemicellulose pyrolysis sub-mechanism and to the elemental composition of the biochar residue.

Table 1 shows the updated multi-step kinetic mechanism, including all the biomass pyrolysis reactions and the kinetic parameters. Together with the hemicellulose pyrolysis improvements, the stoichiomeries of lignin pyrolysis are largely modified mainly to include anisole ($C_6H_5OCH_3$) and vanillin (4-Hydroxy-3-methoxybenzaldehyde: $C_8H_8O_3$) as reference components of lignin tars. The twofold reasons for this modification are that these components are relevant constituents of surrogate mixtures of fast pyrolysis bio-oil [26], and their successive gas phase reactions are investigated [27–29].

This mechanism is also available in CHEMKIN-based format in the Supplemental material, together with the complete list of involved species. Major details on model features are already discussed elsewhere [5]. The multistep kinetic mechanism, based on global and apparent first order reactions, describes the decomposition of each reference component. Volatiles are represented by 29 real and lumped species, including permanent gases and condensable species (tars). Several pyrolysis products are pseudo-species trapped in the metaplastic phase. These are represented as G{..} and are progressively released as volatiles at high temperatures. The solid residue is then represented by pure carbon (CHAR) and the sum of the G{..} species still trapped in the metaplast. The progressive release of these species causes the decrease of biochar yield, the rising of its carbon content, together with a corresponding reduction of oxygen and hydrogen content.

The model accounts for competing reactions that have different selectivities under different temperatures, defining the main path under

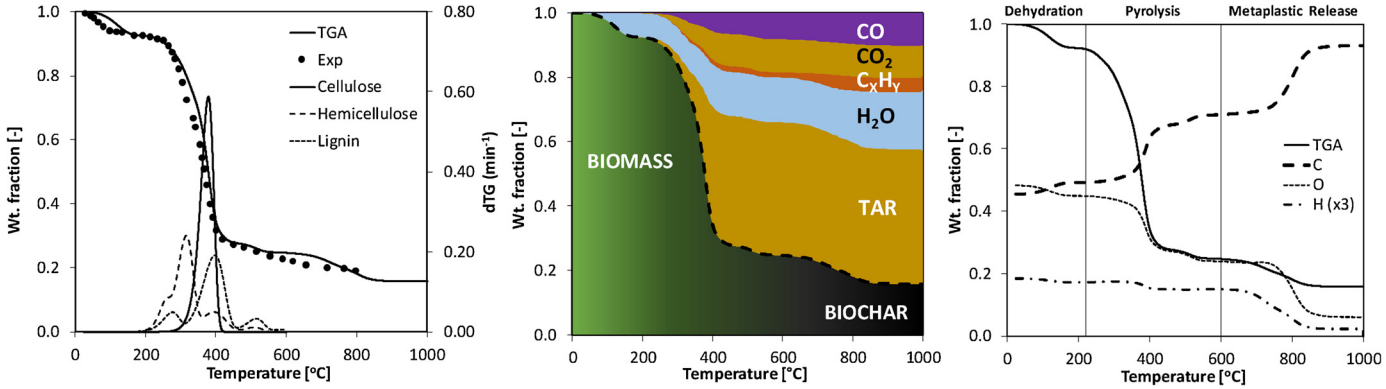

Fig. 2. Pyrolysis of wheat straw at 30 K/min. Left: comparison of predicted and experimental [21] TGA and DTG of reference components. Center: Release of main tar and gas products. Right: Evolution of elemental composition of biochar.

Table 1
Kinetic mechanism of biomass pyrolysis used to obtain the results presented in this work.

Pyrolysis Reactions				Kinetic Parameters A(s^{-1}), Eact (kcal/kmol)
Cellulose				
1	CELL	- >	CELLA	1.50×10^{14} exp(-47000/RT)
2	CELLA	- >	0.05CH2OHCH2CHO + 0.4CH2OHCHO + 0.03CHOCHO + 0.17CH3CHO + 0.25C6H6O3 + 0.35C2H5CHO + 0.2CH3OH + 0.15CH2O + 0.49CO + 0.43CO2 + 0.13H2 + 0.93H2O + 0.02HCOOH + 0.05CH4 + 0.66CHAR + 0.05G{CO} + 0.05G{COH2}$_{Loose}$ + 0.1G{H2}	2.50×10^{6} exp(-19100/RT)
3	CELLA	- >	C6H10O5	3.30 × T × exp(-10000/RT)
4	CELL	- >	0.125H2 + 4.45H2O + 5.45CHAR + 0.12G{COH2}$_{Stiff}$ + 0.25G{CO} + 0.18G{COH2}$_{Loose}$ + 0.125G{H2}	9.00×10^{7} exp(-31000/RT)
Hemicellulose				
5	GMSW	- >	0.7HCE1 + 0.3HCE2	1.00×10^{10} exp(-31000/RT)
6	XYHW	- >	0.35HCE1 + 0.65HCE2	1.25×10^{11} exp(-31400/RT)
7	XYGR	- >	0.12HCE1 + 0.88HCE2	1.25×10^{11} exp(-30000/RT)
8	HCE1	- >	0.06CH2OHCH2CHO + 0.16FURFURAL + 0.1CHOCHO + 0.13C6H6O3 + 0.09CO2 + 0.02H2 + 0.54H2O + 0.25C6H10O5 + 0.1CH4 + 0.25C5H8O4 + 0.1CHAR	16.00 × T × exp(-12900/RT)
9	HCE1	- >	0.4CH2O + 0.49CO + 0.39CO2 + 0.1H2 + 0.4H2O + 0.05HCOOH + 0.1C2H4 + 0.3CH4 + 0.975CHAR + 0.37G{COH2}$_{Stiff}$ + 0.51G{CO2} + 0.01G{CO} + 0.325G{CH4} + 0.075G{C2H4} + 0.43G{COH2}$_{Loose}$ + 0.05G{H2} + 0.2G{C2H6}	3.00 10^{-3} × T × exp(-3600/RT)
10	HCE2	- >	0.145FURFURAL + 0.105CH3CO2H + 0.035CH2OHCHO + 0.3CO + 0.5125CO2 + 0.5505H2 + 0.056H2O + 0.0175HCOOH + 0.049C2H5OH + 0.1895CH4 + 0.7125CHAR + 0.78G{COH2} STIFF + 0.45G{CO2} + 0.105G{CH3OH} + 0.05G{CH4} + 0.1G{C2H4} + 0.18G{COH2}$_{Loose}$ + 0.21G{H2} + 0.2G{C2H6}	7.00×10^{9} exp(-30500/RT)
Lignins				
11	LIGH	- >	0.2CH2OHCHO + 0.5C2H5CHO + 0.1CO + 0.4C2H4 + 0.1C2H6 + LIGOH	6.70×10^{12} exp(-37500/RT)
12	LIGO	- >	CO2 + LIGOH	3.30×10^{8} exp(-25500/RT)
13	LIGC	- >	0.1C6H5OCH3 + 0.22CH2O + 0.21CO + 0.1CO2 + H2O + 0.27C2H4 + 0.1VANILLIN + 0.35LIGCC + 5.85CHAR + 0.4G{COH2}$_{Stiff}$ + 0.36G{CH4} + 0.17G{COH2}$_{Loose}$ + 0.1G{H2} + 0.2G{C2H6}	1.00×10^{11} exp(-37200/RT)
14	LIGCC	- >	0.15C6H5OCH3 + 0.35CH2OHCHO + 1.15CO + 0.7H2 + 0.7H2O + 0.3C2H4 + 0.45CH4 + 0.25VANILLIN + 0.15CRESOL + 0.4C2H6 + 6.8CHAR + 0.4G{CO}	1.00×10^{4} exp(-24800/RT)
15	LIGOH	- >	0.025C24H28O4 + 0.1C2H3CHO + 0.6CH3OH + 0.65CO + 0.05CO2 + H2O + 0.05HCOOH + 0.1CH4 + 0.9LIG + 4.25CHAR + 0.4G{COH2}$_{Stiff}$ + 0.6G{CO} + 0.3G{CH3OH} + 0.25G{CH4} + 0.1G{C2H4} + 0.45G{COH2}$_{Loose}$ + 0.15G{C2H6}	1.50×10^{8} exp(-30000/RT)
16	LIG	- >	0.1C6H5OCH3 + 0.3CH3CHO + 0.6CO + 0.5C2H4 + VANILLIN + 0.1CHAR	4.00 × T × exp(-12000/RT)
17	LIG	- >	0.4CH2O + 0.3CO + 0.1CO2 + 0.6H2O + 0.2CH4 + 6.1CHAR + 0.65G{COH2}$_{Stiff}$ + 0.2G{CO} + 0.4G{CH3OH} + 0.4G{CH4} + 0.5G{C2H4} + 1.25G{COH2}$_{Loose}$ + 0.1G{H2}	8.30×10^{-2} × T × exp (-8000/RT)
18	LIG	- >	0.4CH3OH + 0.4CH2O + 2.6CO + 0.6H2O + 0.75C2H4 + 0.6CH4 + 0.5C2H6 + 4.5CHAR	1.50×10^{9} exp(-31500/RT)
Extractives				
19	TGL	- >	C2H3CHO + 0.5U2ME12 + 2.5MLINO	7.00×10^{12} exp(-45700/RT)
20	TANN	- >	H2O + 0.85C6H5OH + ITANN + G{CO} + 0.15G{C6H5OH}	2.00×10^{1} exp(-10000/RT)
21	ITANN	- >	2CO + H2O + 5CHAR + 0.45G{COH2}$_{Stiff}$ + 0.55G{COH2}$_{Loose}$	1.00×10^{3} exp(-25000/RT)
Metaplastic				
22	G{CO2}	- >	CO2	1.00×10^{6} exp(-24500/RT)
23	G{CO}	- >	CO	5.00×10^{12} exp(-52500/RT)
24	G{CH3OH}	- >	CH3OH	2.00×10^{12} exp(-50000/RT)
25	G{COH2}$_{Loose}$	- >	0.2CO + 0.2H2 + 0.8H2O + 0.8CHAR	6.00×10^{10} exp(-50000/RT)
26	G{C2H6}	- >	C2H6	1.00×10^{11} exp(-52000/RT)
27	G{CH4}	- >	CH4	1.00×10^{11} exp(-53000/RT)
28	G{C2H4}	- >	C2H4	1.00×10^{11} exp(-54000/RT)
29	G{C6H5OH}	- >	C6H5OH	1.50×10^{12} exp(-55000/RT)
30	G{COH2}$_{Stiff}$	- >	0.8CO + 0.8H2 + 0.2H2O + 0.2CHAR	1.00×10^{9} exp(-59000/RT)
31	G{H2}	- >	H2	1.00×10^{8} exp(-70000/RT)
H_2O Evaporation				
32	ACQUA	- >	H2O	1 × T × exp(-8000/RT)

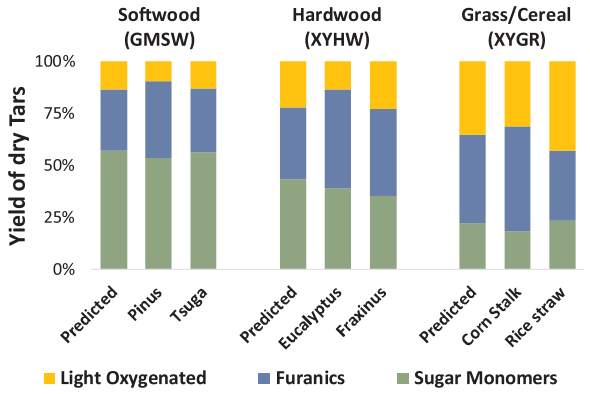

Fig. 3. Distribution of condensable products of hemicellulose from different types of biomass. Comparison between predicted (GMSW, XYHW, XYGR) and experimental data of Softwood (Pinus, Tsuga), Hardwood (Eucalyptus, Fraxinus) [31] and Grass/Cereals (Corn stalk, rice straw) [30].

low and high temperatures. These features are present for the reference components of cellulose, hemicellulose and lignin, while extractives were not accounted for these differences because of their reduced amount in the samples and less importance in the global biomass pyrolysis. In general, the low temperature mechanisms produce more biochar and gases, while high temperature yield more tars.

A few examples of the hemicellulose pyrolysis are here reported, showing the improvements on characterization and kinetics proposed, and highlighting the flexibility of the model. Fig. 3 shows the distribution of tar species produced from the pyrolysis of the three different hemicelluloses at 550 °C, and also satisfactorily compares model predictions with the experimental data of Wang et al [30,31] in terms of sugars, furanic and light oxygenated species. The Authors applied an improved method using detergents for hemicellulose extraction, without relevant structure damage and low-ash content extracted samples, when compared to commercial available hemicellulose model compounds. The comparisons highlight the higher sugar monomers release from softwood, and the higher content of light oxygenated from grass/cereals. This is the consequence of the higher presence of 6-carbon sugar monomers and less branched structure of softwood hemicellulose (HCE1). The 6-carbon sugars are more easily released as anhydrous monomers, more similar to the decomposition of cellulose, while 5-carbon sugars tend to decompose into furanics and light oxygenated compounds (HCE2).

In order to highlight the different behavior of softwood, hardwood, and grass hemicellulose, Fig. 4 compares TGAs at 20 K/min, and it shows the difference in final solid residues as well reactivities of the three samples. The experimental data of Glucomannan and Xylan represent the average experimental data already discussed in [5], and they are compared to the predictions of GMSW and XYHW pyrolysis, respectively. Hemicellulose extracted from rice straw and corn stalk [30] are compared to the XYGR pyrolysis predictions. This variability in hemicellulose structures and decomposition was not considered and simply averaged in the previous kinetic models [2008; 2015]

The improvements proposed are further validated in Fig. 5, where comparisons between experimental and predictions of mass loss during torrefaction of xylan are analyzed in a temperature range of 200–300 °C, with a successive pyrolysis up to 700 °C. The mass losses are reported as a function of temperature [32] and reaction time [33]. Simulations refer only to the first 120 min under inert atmosphere, whereas the experiment proceeds with the final oxidation step. Fig. 6 shows comparison of predictions and experimental data on solid, gas and tar, together with CO and CO_2 yields for xylan pyrolysis [34] from

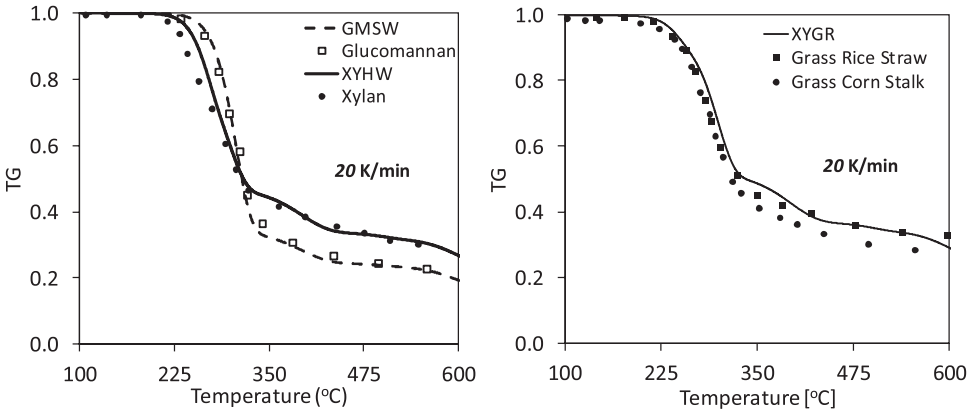

Fig. 4. Pyrolysis of glucomannan, xylan [5] and hemicellulose extracted from grass/cereal [30].

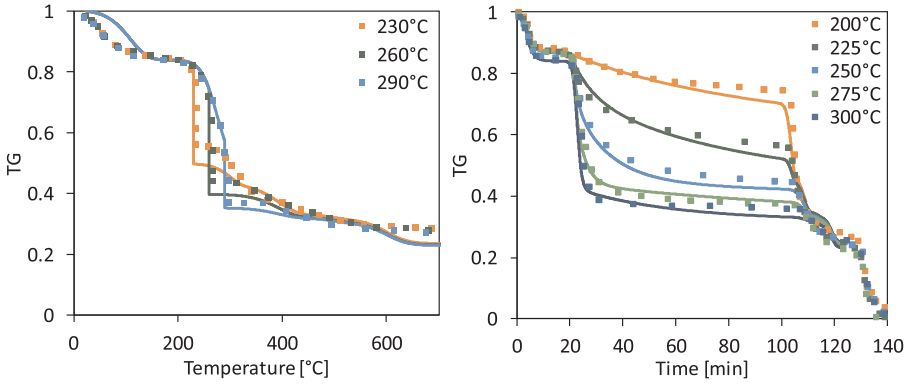

Fig. 5. Torrefaction of Xylan. Mass loss versus temperature program [32], and versus reaction time [33].

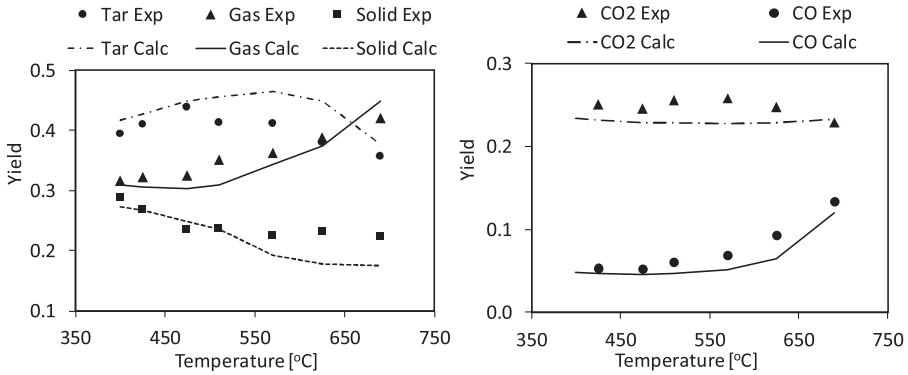

Fig. 6. Xylan pyrolysis. Yield of biochar, gas and tars, CO and CO2 [34].

Table 2
Biomass elemental composition and characterization in terms of reference components. Spruce wood, birch wood [38], peanut shell [39], waste wood shavings [40], and maple wood [41].

Mass Fraction	Spruce Wood	Birch Wood	Peanut Shell	Waste Wood	Maple Wood
Elemental composition					
C (daf)	0.498	0.478	0.484	0.467	0.534
H (daf)	0.064	0.064	0.062	0.058	0.068
O (daf)	0.438	0.458	0.454	0.474	0.398
Ash (dry)	0.007	0.006	0.017	0.015	0.017
Characterization					
CELL	0.482	0.555	0.579	0.519	0.251
XYHW	–	0.303	0.202	–	0.205
GMSW	0.262	–	–	0.181	–
LIGO	0.001	0.000	0.046	0.116	0.002
LIGH	0.173	0.072	0.097	0.004	0.349
LIGC	0.026	0.011	0.021	0.018	0.051
TANN	0.000	0.000	0.010	0.070	0.001
TGL	0.049	0.050	0.028	0.001	0.089
Moisture	–	0.030	–	0.075	0.035
ASH	0.007	0.006	0.017	0.015	0.017

400 to 700 °C. The model follows the experiments trends: tars exhibit a maximum yield at ~450 °C, where devolatilization is almost complete. At higher temperatures, tar yield reduction is caused by the progressive importance of secondary gas-phase-reactions (tar cracking), leading to increase in gas yields. In order to obtain these results, the reference component XYHW was first pyrolyzed following the kinetic mechanism proposed in this work, followed by processing the volatiles released with the CRECK detailed gas-phase reactions mechanism [14], using the temperature and residence times mentioned by the author Shen, et al. [34]. The detailed mechanism includes +500 species and +18,000 reactions. The residence time in the reactor was about 0.5–1 s, which is long enough to increase CO and light gases yield, mainly above 650 °C. These simulation examples related to hemicellulose emphasized the main novelties of the CRECK model accounted for both the characterization and the primary pyrolysis reactions.

The very recent work of Zhou, et al. [35] discusses and proposes a mechanistic model for fast pyrolysis of hemicellulose from corn stover, with 504 reactions of 114 species, based on quantum chemical calculations. They also observe large difference between pyrolysis products from native and extracted hemicelluloses, mainly caused by the severe extraction treatments, which damage the original structure. This and similar more detailed works [20,36,37] clearly point out the complexity of the biomass pyrolysis mechanisms. However, more practical engineering investigations at the particle and the reactor scale require strong simplifications. Therefore, the CRECK lumped pyrolysis mechanism seems more adequate and satisfactory for these applications.

The improvements and modifications related to the release of metaplastic species and biochar composition are discussed in the next Section.

3. H/C/O composition of biochar and model validation

All the selected biomass samples taken from the database were first characterized in terms of reference species, based on the biochemical composition either specified or calculated. Then the biomass pyrolysis model predicts the time evolution of the yield and composition of the residual biochar, according to the specified operating conditions. As said, the predicted solid residue (biochar) is the sum of the fixed carbon (CHAR) and all the residual lumped species (G{..}) still trapped in metaplastic phase. H/C/O composition of the biochar is calculated simply taking into account mass fraction and composition of each residual species. To better show the model performance, feedstock composition and characterization of some biomass samples are reported in Table 2. Figs. 7 and 8 show the corresponding comparisons between experimental data and model predictions. In Fig. 8, no experimental data on yield of solids were reported, so we report only the calculated values.

These examples refer to:

- TGA torrefaction of spruce (softwood) and birch (hardwood) biomass samples at temperatures from 220 to 300 °C, at heating rate of 40 °C/min, for 2 h [38] (Fig. 7);
- Pyrolysis of peanut shell in a fixed bed reactor heated by electrical furnace at 15 °C/min [39] (Fig. 8a);
- Pyrolysis of waste wood shavings in a fluidized bed reactor at different constant temperatures [40] (Fig. 8b);
- Pyrolysis of Maple wood shavings in a stainless steel tube furnace at temperatures from 300 to 700 °C [41] with heating rates of 25 °C /min (Fig. 8c);

As temperature rises, the oxygen and hydrogen content drops, caused by the breakage of weaker bonds releasing light gases, resulting in a reduction of the biochar yield and an increase of the carbon content. This effect is less evident in the torrefaction process, whereas it is very clear in the high temperature pyrolysis treatments shown in Fig. 8. To highlights the improvements of the new kinetic model, the comparisons with the previous version of the pyrolysis mechanism are reported in the Supplemental Material.

As already mentioned, the biomass pyrolysis model has been modified, especially with respect to the release of metaplastic species, in order to better agree with experimental data of biochar yields and H/C/O composition. Biochar structures and functional groups were studied by several authors [41–44], typically supported by solid state C-13 NMR (Nuclear Magnetic Resonance) and Raman spectroscopy. A wide range of functionalities, whose distribution depends on the sample composition, characterizes the structure of the raw biomass. The typical bands detected in NMR spectra of biomass indicate groups of aliphatic carbon (primary, secondary and tertiary), carbonyl, carboxyl, aldehyde/ketone, methoxyl, methylene, methyl acetates, protonated and non-protonated aromatics, and aromatics linked with methoxyl groups

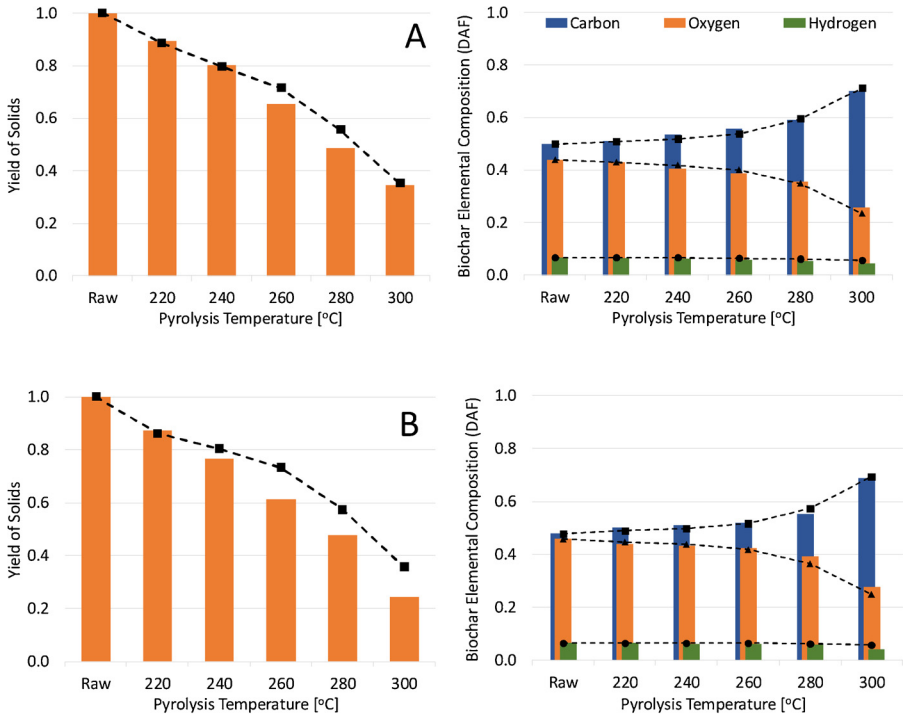

Fig. 7. Torrefaction of (A) Spruce (Softwood) and (B) Birch (Hardwood) [38]. Comparison of experimental data (bars) and model predictions (lines) in terms of biochar yield and composition vs pyrolysis temperature.

and with oxygen [41]. Biomass components, cellulose, hemicellulose, lignin, and extractives have characteristic functional groups, which can be identified in these bands. Along with the decomposition of these components, their characteristic bands reduce in intensity, increasing the band intensity of biochar characteristic structures: aliphatics, and aromatic C—H, C—O, C—O—C, and C—C. The formation of aliphatic carbon is typical in pyrolysis at 300–350 °C when most of the sugar structures of cellulose and hemicellulose already decomposed. Carboxyl, carbonyl and acetates bands quickly diminish with increasing pyrolysis temperature. Aliphatic carbon bands significantly reduce after 400 °C with the release of light hydrocarbons, because of the breakage of weaker bonds in the forming biochar. Progressively, the size of aromatic clusters grows with the loss of C—H, C—O and C—O—C aromatic groups, increasing C—C aromatic bands, as non-edge carbon.

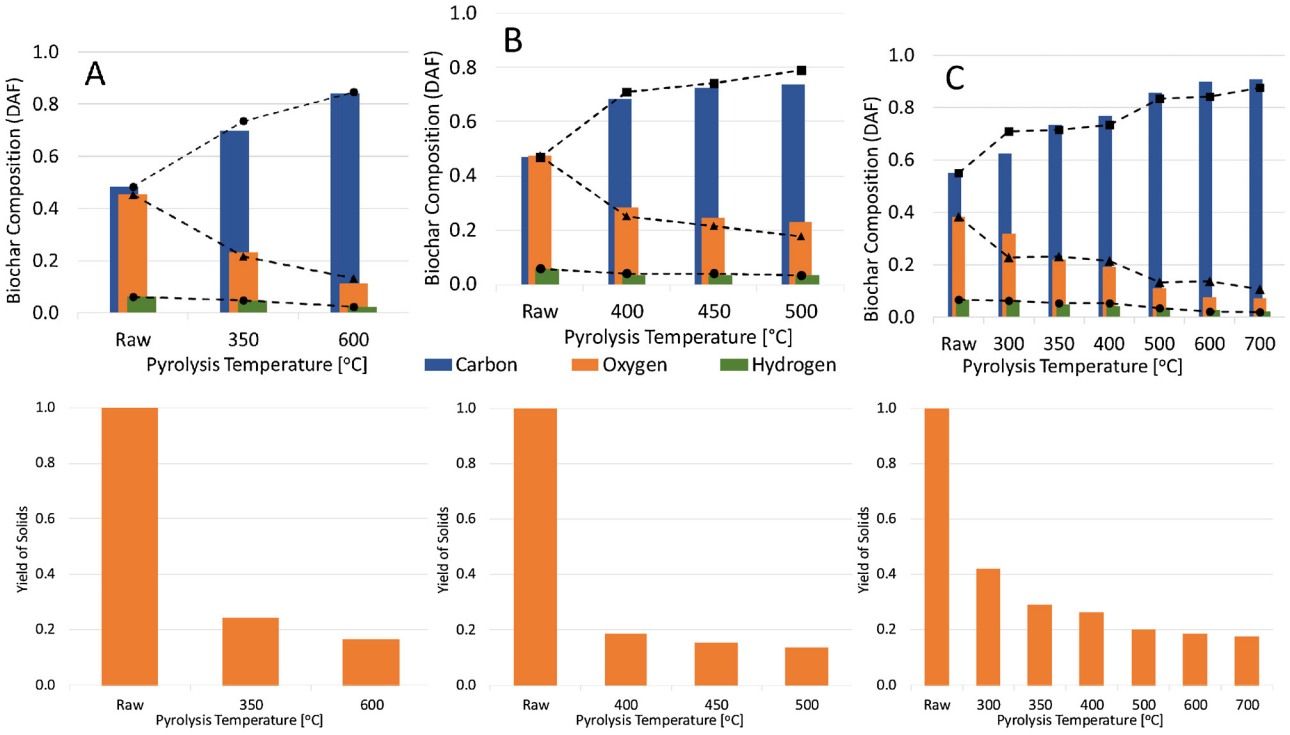

Fig. 8. Pyrolysis of peanut shell (A) [39], waste wood shavings (B) [40], and maple wood (C) [41]. Comparison of experimental data (bars) and model predictions (lines).

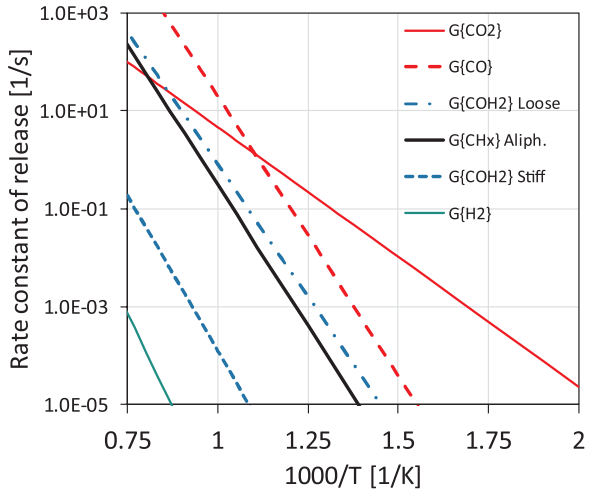

Fig. 9. Rate constant of the release of metaplastic species.

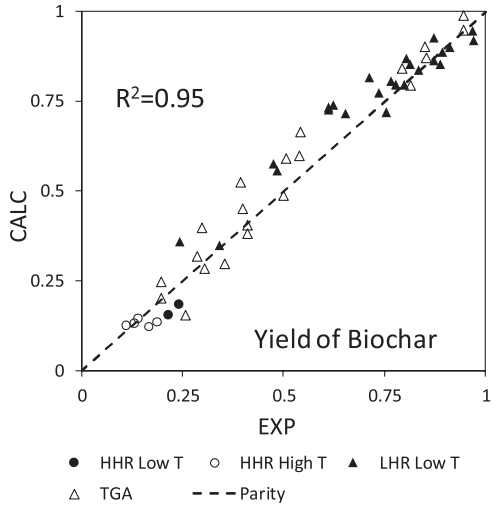

Fig. 10. Parity diagram of experimental and predicted values of biochar yield.

These are the preliminary steps describing the biomass evolution to a less ordered biochar; then, there is a progressive ordering of aromatic clusters to more turbostratic and graphitic-like structures. Cao, et al. [41] measured clusters with about 20, 40, 60 and 80 carbon atoms for pyrolysis of maple wood at 400, 500, 600 and 700 °C, respectively. Moreover, Brewer, et al. [42] report significant differences in the functional groups found for pyrolysis performed under low and high heating rates. The low heating process allowed to reach more ordered structures with higher carbon content, because of a more complete release of the weaker bonded groups. The slow pyrolysis experiments at 500 °C produced a biochar with 40% larger clusters (16 vs. 23 C atoms), when compared to the fast pyrolysis at the same temperature [42]. This fact further confirms that the structural evolution of the biochar, and its composition, is not only sensitive to temperature, but also on operating conditions.

The CRECK pyrolysis model describes the residual biochar with a pure carbon species (CHAR) together with several lumped metaplastic species. The release of these lumped species should take into account and respect this structural information. Some similar modifications of the scheme, mainly intended to reduce the release rate of metaplastic species at high temperatures, were also proposed by Anca-Couce for large biomass particles [45].

Fig. 9 schematically shows the updated rate of release of metaplastic species in the temperature range 500–1333 K. The lumped oxygenated species G{CO2}, G{CH3OH} and G{CO}, representing alcohol/aldehyde/ketone/carboxylic acid functional groups, are first released. G{CH3OH} and G{CO} species are released with very similar rates. For keeping the easy reading of the plot, we report only the G{CO}. For the same reason, G{C6H5OH} is not reported, having a similar releasing rate as $G\{COH2\}_{Loose}$. Then, the aliphatic carbon groups G{CH4}, G{C2H6}, and G{C2H4} follow, together with the release of $G\{COH2\}_{Loose}$ group. G{H2} and the stiff G{COH2} groups, with different releasing rates, describe the final oxygen and hydrogen content in the residual biochar. Whereas the $G\{COH2\}_{Loose}$ group release mainly H2O with a charification process, the stiff G{COH2} group contributes to the final release of CO and H2, gases detected typically at high temperature during biomass pyrolysis. In fact, as shown in Fig. 9, the final release of metaplastic species $G\{COH2\}_{Stiff}$ and G{H2} groups typically takes place only at temperatures higher than 1400 K and 1800 K, respectively, where their half life time is about 1 s. This progressive release of these last two metaplastic species globally agrees with the decrease of C–H, and the increase of C—C bond bands in NMR. In Raman spectroscopy, the IV, ID and IG bands refer to amorphous, large aromatic cluster with defects, and graphitic biochar structures, respectively. The decrease of IV band reflects the devolatilization of weakly bonded functionalities, while the increase of ID bands refers to the reordering of smaller aromatic clusters, forming a larger carbonaceous structure. The IG band does not increase because the pyrolysis temperature does not reach graphitization temperature and time. Therefore, the evidences found by NMR analysis are reinforced by Raman spectroscopy findings, showing a strong decrease of IV/ID ratios at lower temperatures and an increase of ID/IG at higher temperatures [44].

The parity diagrams in Figs. 10 and 11 show the whole set of comparisons (80 samples). In order to better analyze these data, experiments are first divided into:

- Low heating rate (LHR): experiments in TGA and reactors with programmed heating rate.
- High heating rate (HHR): experiments in fluidized bed, drop tube, pyroprobe and similar devices.

Both these categories are further subdivided depending on low and high final temperature (550 °C is the threshold temperature). Finally, TGA category refers to TGA experiments in which H/C/O data of biochar is not provided.

A correct prediction not only of biochar yield, but also its elemental composition is of utmost importance, because it strongly affects successive biochar reactivity in combustion and gasification processes [46]. The elemental composition is only a first feature because it is indeed necessary to define correctly the oxygenated and aliphatic surface functionalities, the catalytic active sites as well as the porosity and specific surface [41,47].

These comparisons show that the model is capable of significantly improving the prediction of both biochar yield and its composition at several different temperatures and heating conditions. These results obtained with previous version of the kinetic scheme are reported in the supplemental material, revealing the improvements, mostly in the R^2 correlation index, which is now higher than 90% for all these predictions, and the absence of systematic deviations. This fact is well evident in Fig. 12, where the residuals (experimental – predictions) are reported as a function of the temperature. Larger hydrogen residuals are present at low temperatures, also because of a higher sensitivity of model results to operating and simulation parameters. Moreover, this fact is not anymore true when considering relative instead of absolute errors.

As already discussed, these results have been obtained after a specific tuning of the pyrolysis model, mainly with respect to the formation and release of metaplastic species (see Fig. 9). The tuning activity proposed in this model significantly improved the R^2 correlation indexes. However, some scatter still persists caused not only by the large simplifications of the biomass characterization and the pyrolysis model,

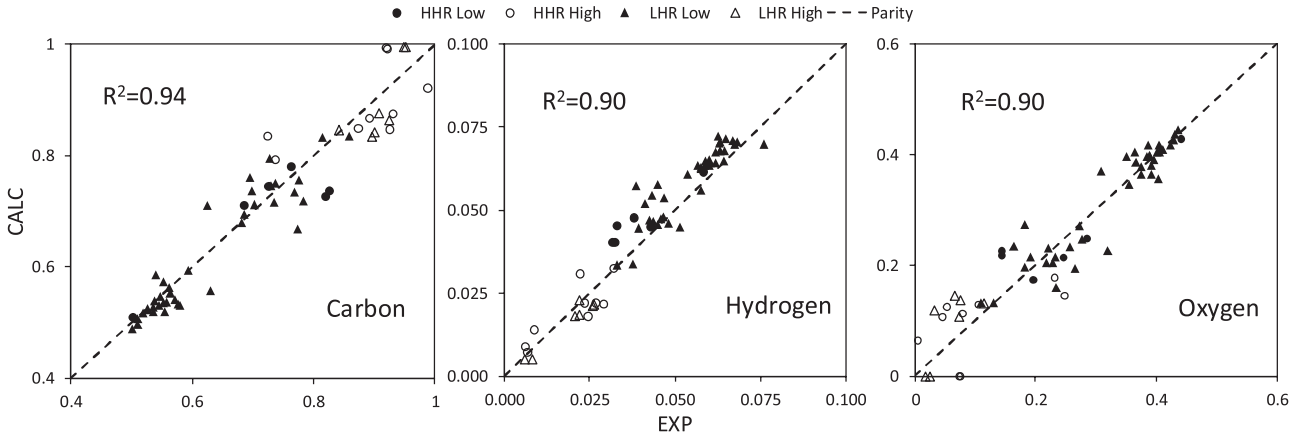

Fig. 11. Parity diagrams of experimental and predicted values of biochar elemental composition.

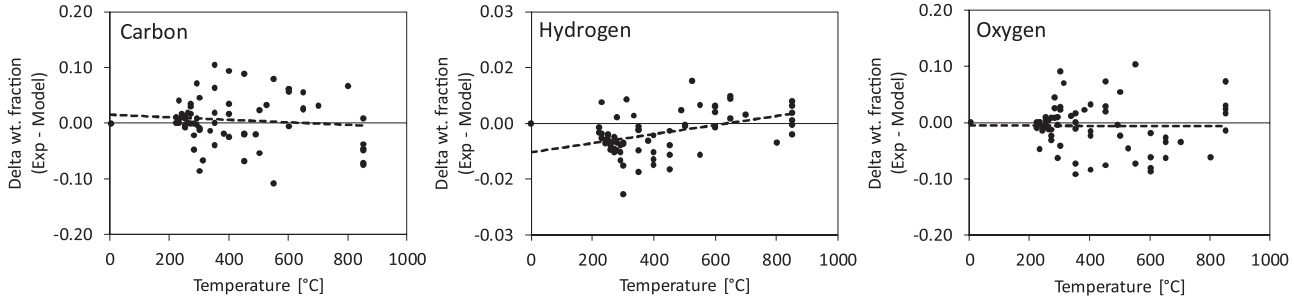

Fig. 12. Distribution of residuals (experimental-prediction) of elemental composition and yields of biochar vs peak pyrolysis temperature.

but also to the experimental uncertainties, including the poor knowledge of the biomass origin and composition, and the incomplete description of the reactors and operating conditions.

Moreover, the scatter of the HHR experiments in Fig. 10 highlights a minor systematic biochar underpredictions, whereas an opposite deviation is observed for the LHR data. At high temperatures and high heating rates, the release of metaplastic species should be partially reduced. Jia, et al. [48] also reached similar conclusions, when investigating the performance of our previous model on a fluidized and a fixed bed reactor. Although the predictions of the improved pyrolysis model better agree with experiments at low and intermediate temperature conditions, there is still space to further develop the HHR predictions, typical of fluidized bed reactors.

4. Sensitivity analysis

A sensitivity analysis with respect to cellulose and hemicellulose decomposition (Reactions 2, 4 and 9) was already discussed in the previous paper [5], when discussing the catalytic effect of ash. The increase of reaction rates of these reactions reduces levoglucosan and xylan in favor of decomposition and dehydration products, along with a char yield increase. As far as lignins and the release of metaplastic species are concerned, Fig. 13 shows a couple of simple examples of model sensitivity to reaction rate parameters. For these purposes, the pyrolysis of a milled grass/cereal lignin (*Miscanthus sinensis*) [49] is analyzed. At low temperatures (T < 600 °C), pyrolysis of this biomass is mainly affected by the selectivity among competitive reactions of lignin degradation (reactions 16–18 in Table 1), as well as by their

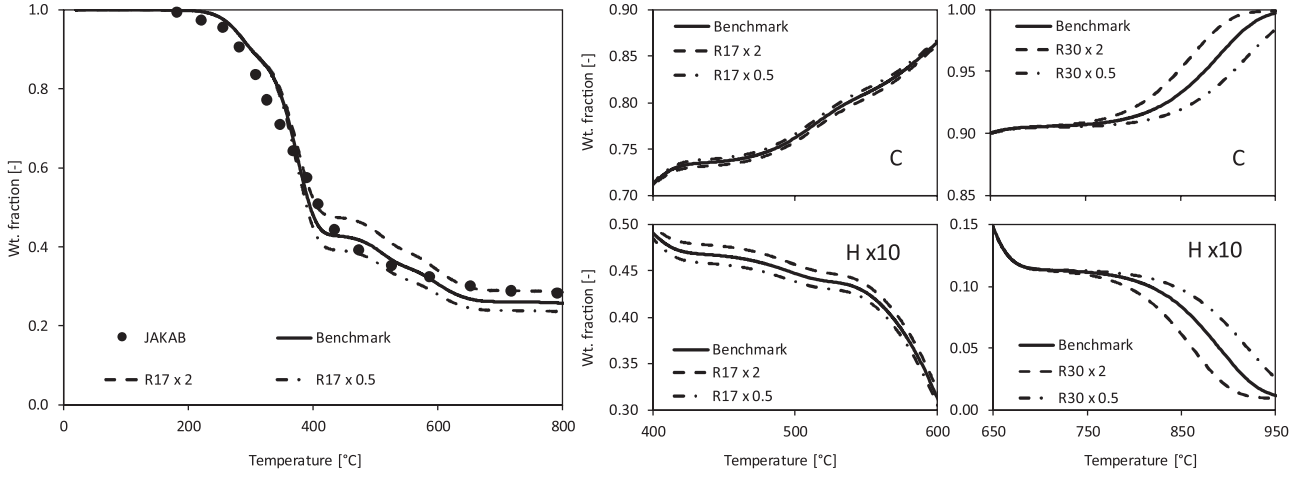

Fig. 13. Sensitivity analysis. Residue and biochar carbon and hydrogen content. Reactions 17 and 30 refer to Table 1.

stoichiometries. On the other hand, the release of metaplastic species plays a major role on biochar composition at high temperatures.

Thus, as a first example the sensitivity to reaction 17 is analyzed with the brute force method. Biochar yield increases, while carbon content decreases, because the doubling of the rate constant promotes the formation of metaplastic species, and reduces the release of tar components. This effect is clearly confirmed by the higher amount of biochar residue in the TGA curve. Moreover, only at higher temperatures (T > 700 °C) biochar composition is affected by the release of $G\{COH_2\}_{Stiff}$ (reaction 30). Therefore, biochar residue turns out to increase C content and deplete both H and O concentration, as doubling this reaction rate. These analyses clearly confirm that the kinetic parameters tuned in this work are much more sensitive to the composition than to the yield of biochar. Therefore, upgrading the CRECK kinetic mechanism aiming to improve biochar composition did not affect the previous agreements [5,8,19,20,23]. As a final comment to the sensitivity analysis, it is clear that the rate and stoichiometry of the first decomposition steps mainly affect the tar and gas product distributions, whereas the formation and release of metaplastic species drives the biochar yield and composition.

5. Conclusion

The present work provides a collection of a large set of experimental data, which was organized in a database containing biomass and biochar compositions, together with the experimental operating conditions. This database allows a better understanding of the evolution of biochar yield and composition, from several biomasses under different pyrolysis conditions. This kinetic investigation allowed a further tuning of CRECK multistep kinetic mechanism of biomass pyrolysis [5] leading to a better characterization of yields and composition of residual biochar. The yield is an important factor for the optimal design of thermal conversion reactors, while biochar elemental composition strongly influences its reactivity in gasification and oxidation environments. Improvements in biochar predictions represent a crucial step towards the ongoing research activity on heterogeneous reactions of biochar gasification and combustion. The characterization of char composition in a broader range of conditions, accounting for the influence of transport resistances and cross-linking (also called secondary charification) reactions, will be addressed in a future work more completely describing mass and energy balance equations at the particle and reactor scales [22]. It is important to highlight that the biomass pyrolysis model remains a simple but flexible approach to describe the complex behavior of pyrolysis products. Despite these simplifications, this model is the only one, to our knowledge, able to describe in a comprehensive and predictive way the chemistry of the whole process from biomass to thermochemical conversion products, providing interesting details with little computational cost.

Acknowledgements

P.D. gratefully acknowledges the financial support from CAPES Foundation, Ministry of Education of Brazil–Science without Borders Mobility Program–Full PhD Scholarship Process No. 10131/13-2.

Appendix A. Supplementary data

Supplementary material related to this article can be found, in the online version, at doi:https://doi.org/10.1016/j.jaap.2018.06.022.

References

[1] L. Brennan, P. Owende, Renew. Sustain. Energy Rev. 14 (2010) 557.
[2] G. Dragone, B.D. Fernandes, A.A. Vicente, J.A. Teixeira, Curr. Res., Technol. Educ. Topics Appl. Microbiol. Microb. Biotechnol. 2 (2010) 1355.
[3] K. Ullah, M. Ahmad, V.K. Sharma, P. Lu, A. Harvey, M. Zafar, S. Sultana, C. Anyanwu, Prog. Nat. Sci.: Mater. Int. 24 (2014) 329.
[4] P. Chen, M. Min, Y. Chen, L. Wang, Y. Li, Q. Chen, C. Wang, Y. Wan, X. Wang, Y. Cheng, Int. J. Agric. Biol. Eng. 2 (2010) 1.
[5] E. Ranzi, P.E.A. Debiagi, A. Frassoldati, ACS Sustain. Chem. Eng. 5 (2017) 2867.
[6] A.V. Bridgwater, Biomass Bioenergy 38 (2012) 68.
[7] A. Demirbas, J. Anal. Appl. Pyrolysis 72 (2004) 243.
[8] E. Ranzi, P.E.A. Debiagi, A. Frassoldati, ACS Sustain. Chem. Eng. 5 (2017) 2882.
[9] O. Senneca, P. Salatino, Proc. Combust. Inst. 33 (2011) 1763.
[10] As. Anca-Couce, A. Dieguez-Alonso, N. Zobel, A. Berger, N. Kienzl, F. Behrendt, Energy Fuel 31 (2017) 2335.
[11] D. Neves, H. Thunman, A. Matos, L. Tarelho, A. Gómez-Barea, Prog. Energy Combust. Sci. 37 (2011) 611.
[12] A. Anca-Couce, Prog. Energy Combust. Sci. 53 (2016) 41.
[13] T. Kan, V. Strezov, T.J. Evans, Renew. Sustain. Energy Rev. 57 (2016) 1126.
[14] P.E.A. Debiagi, G. Gentile, M. Pelucchi, A. Frassoldati, A. Cuoci, T. Faravelli, E. Ranzi, Biomass Bioenergy 93 (2016) 60.
[15] A. Anca-Couce, R. Mehrabian, R. Scharler, I. Obernberger, Energy Convers. Manage. 87 (2014) 687.
[16] A. Gómez-Barea, B. Leckner, Prog. Energy Combust. Sci. 36 (2010) 444.
[17] A.D. Paulsen, M.S. Mettler, P.J. Dauenhauer, Energy Fuel 27 (2013) 2126.
[18] P.E.A. Debiagi, C. Pecchi, G. Gentile, A. Frassoldati, A. Cuoci, T. Faravelli, E. Ranzi, Energy Fuel 29 (2015) 6544.
[19] E. Ranzi, A. Cuoci, T. Faravelli, A. Frassoldati, G. Migliavacca, S. Pierucci, S. Sommariva, Energy Fuel 22 (2008) 4292.
[20] T. Faravelli, A. Frassoldati, G. Migliavacca, E. Ranzi, Biomass Bioenergy 34 (2010) 290.
[21] V. Pasangulapati, Devolatilization Characteristics of Cellulose, Hemicellulose, Lignin and the Selected Biomass During Thermochemical Gasification: Experiment and Modeling Studies, State University, Oklahoma, 2012 p..
[22] E. Ranzi, M. Corbetta, F. Manenti, S. Pierucci, Chem. Eng. Sci. 110 (2014) 2.
[23] M. Corbetta, A. Frassoldati, H. Bennadji, K. Smith, M.J. Serapiglia, G. Gauthier, T. Melkior, E. Ranzi, E.M. Fisher, Energy Fuel 28 (2014) 3884.
[24] H. Bennadji, K. Smith, S. Shabangu, E. Fisher, Pittsburgh, PA, USA, AIChE Annual Meeting, International Congress on Energy (ICE) (2012).
[25] K. Dussan, S. Dooley, R. Monaghan, Chem. Eng. J. 328 (2017) 943.
[26] Horizon2020, in, H2020 Research and Innovation Action, 2016-2019.
[27] E.B. Hemings, G. Bozzano, M. Dente, E. Ranzi, Chem. Eng. Trans. 24 (2011) 61.
[28] M. Nowakowska, O. Herbinet, A. Dufour, P.-A. Glaude, Combust. Flame 161 (2014) 1474.
[29] M. Pelucchi, C. Cavallotti, A. Cuoci, T. Faravelli, A. Frassoldati, E. Ranzi, Energy Environ. Sci. (2018) (Submited).
[30] S. Wang, B. Ru, G. Dai, W. Sun, K. Qiu, J. Zhou, Bioresour. Technol. 190 (2015) 211.
[31] S. Wang, B. Ru, H. Lin, W. Sun, Fuel 150 (2015) 243.
[32] W.-H. Chen, P.-C. Kuo, Energy 36 (2011) 803.
[33] W.-H. Chen, P.-C. Kuo, Energy 36 (2011) 6451.
[34] D. Shen, S. Gu, A.V. Bridgwater, J. Anal. Appl. Pyrolysis 87 (2010) 199.
[35] X. Zhou, W. Li, R. Mabon, L.J. Broadbelt, Energy Environ. Sci. (2018).
[36] R. Vinu, L.J. Broadbelt, Energy Environ. Sci. 5 (2012) 9808.
[37] X. Zhou, H.B. Mayes, L.J. Broadbelt, M.W. Nolte, B.H. Shanks, AlChE J. 62 (2016) 766.
[38] Q.-V. Bach, W.-H. Chen, Y.-S. Chu, Ø. Skreiberg, Bioresour. Technol. 215 (2016) 239.
[39] P.R. Bonelli, Energy Sour. 25 (2003) 767.
[40] P.A. Horne, P.T. Williams, Fuel 75 (1996) 1051.
[41] X. Cao, J.J. Pignatello, Y. Li, C. Lattao, M.A. Chappell, N. Chen, L.F. Miller, J. Mao, Energy Fuel 26 (2012) 5983.
[42] C.E. Brewer, K. Schmidt-Rohr, J.A. Satrio, R.C. Brown, Environ. Prog. Sustain. Energy 28 (2009) 386.
[43] Y. Le Brech, J. Raya, L. Delmotte, N. Brosse, R. Gadiou, A. Dufour, Carbon 108 (2016) 165.
[44] C. Guizani, K. Haddad, L. Limousy, M. Jeguirim, Carbon 119 (2017) 519.
[45] A. Anca-Couce, P. Sommersacher, R. Scharler, J. Anal. Appl. Pyrolysis 127 (2017) 411.
[46] M. Morin, S. Pécate, M. Hémati, Y. Kara, J. Anal. Appl. Pyrolysis 122 (2016) 511.
[47] J. Lee, K.-H. Kim, E.E. Kwon, Renew. Sustain. Energy Rev. 77 (2017) 70.
[48] L. Jia, A. Dufour, Y. Le Brech, O. Authier, G. Mauviel, Chem. Eng. J. 313 (2017) 270.
[49] E. Jakab, O. Faix, F. Till, J. Anal. Appl. Pyrolysis 40 (1997) 171.